Computational fluid dynamic simulations of solidification for enhancing speed of continuous cast copper

Jones, Thomas D. A.; Strachan, Richard I.; Mackie, David M.; Cooper, Mervyn; Frame, Brain; Vorstius, Jan B.

DOI:
10.1016/j.jestch.2020.12.009

Publication date:
2021

Document Version
Publisher's PDF, also known as Version of record

Engineering Science and Technology, an International Journal 24 (2021) 92–104

HOSTED BY

Contents lists available at ScienceDirect

Engineering Science and Technology, an International Journal

journal homepage: www.elsevier.com/locate/jestch

Computational fluid dynamic simulations of solidification for enhancing speed of continuous cast copper

Thomas D.A. Jones [a,*], Richard I. Strachan [a,b], David M. Mackie [a], Mervyn Cooper [b], Brain Frame [b], Jan B. Vorstius [a]

[a] University of Dundee, School of Science and Engineering, Dundee DD1 4NH,UK
[b] Rautomead Ltd, Dundee DD2 4UH, UK

ARTICLE INFO

Article history:
Received 14 July 2020
Revised 17 November 2020
Accepted 2 December 2020

Keywords:
Casting
Copper alloy
Computational fluid dynamic
Simulation
Solidification
Grain structure

ABSTRACT

In this research experiment computational fluid dynamic (CFD) models were constructed, within Ansys Fluent TM v.R1, to investigate phenomena occurring during the Vertically Upwards Continuous Casting (VUCC) of 8 mm diameter, oxygen free copper (OFCu) for alterations to the casting speed. The simulated influence of heat transported over a 0.1 mm air gap formed within the casting die was investigated and a value for the die wall heat transfer coefficient (hc) of $(9.0 \pm 0.2) \times 10^4$ W/m^{2}K, was extracted. Using this value for hc, simulations of the entire casting crucible and die were made for casting speed settings: pushback motion at 0.06 m/s, average; dwell motion (pause) at 0.05 m/s, average; and continuous motions at 0.022 m/s, 0.015 m/s and 0.008 m/s; and were validated against literature values for measured thermal distribution within the casting die. The fastest casting speed for 8 mm OFCu was investigated and a trend between simulated solidification front and measured grain growth direction was identified, highlighting, the casting motions pushback and dwell yield improved casting conditions. Fluid flow rate was investigated within the casting crucible and showed a small influence on casting due to natural convection relative to flow within the die, 0.001 ± 0.0005 m/s compared with 0.1 ± 0.01 m/s for pushback casting, respectively.

1. Introduction

Copper metal of purity greater than 99.999%, is referred to as oxygen-free copper (OFCu) and is mainly applied within the automotive and energy sectors, with other applications including high conductivity materials for data communication, super conducting magnets for particle accelerators and enamelled wire [1]. The growth of OFCu demand is mainly driven by developments in electrical vehicles and electrical device manufacture. The continuous casting process is the most common technique used to produce by-the-tonne volumes of high purity, high quality OFCu metal at casting speeds of approximately 100 kg/hour or ~ 4 m/min [2]. Continuous casting of metal rods or sheets can be performed horizontally [3] or by Vertically Upward Continuous Cast (VUCC) [4,5]. VUCC of OFCu yields the highest quality with minimal defects, for average casting speeds of 100 kg/hr [6]. VUCC shows benefits over horizontal casting orientation due to increased cooling rates within the solidification process, which enable desirable reductions to grain structure size [7] and lower defects [8]. In casting, the formation of grains of micro-scale size is attributed to higher strength cast pieces, which are desirable for manufacturing as they enable increased performance [9] and yield [10].

Metal solidification is influenced by casting parameters such as withdraw speed (m/s or kg/hr), diameter of desired cast rod and heating extracted to the casting setup. Of importance during VUCC is the application of pushback and dwell (a pause of the motion), to the cast rod which enables improved casting conditions [11]. The application of pushback or dwell motions is typically applied in manufacture [12] and enables access to faster casting speeds. Their application is required when casting at the fastest speeds (3 – 4 m/min) and is approximately the maximum speed at which high quality cast OFCu can be obtained for this configuration, as quantified by Rautomead Ltd [5]. This is due to higher speeds introducing greater heat into the casting die [4] which results in poorer solidification and breakage of the rod. The application of both dwell and pushback motions is attributed with improved consistency of the cast rod structure, however, a complete understanding of their

* Corresponding author.
E-mail address: t.d.a.jones@dundee.ac.uk (T.D.A. Jones).
Peer review under responsibility of Karabuk University.

https://doi.org/10.1016/j.jestch.2020.12.009
2215-0986/

influence is lacking, which this research aims to increase and remedy.

Recent developments within computational fluid dynamic (CFD) software has enabled in-depth modelling of the thermal and fluid motions occurring within a casting rig, which can be used to identify conditions for high quality manufacturing [13,14] and casting manufacturing [15,16]. CFD simulation can model solidification using the enthalpy porosity method, which highlights the position where solidification occurs from the liquid to the solid cast piece, referred to as the solidification front (SF) [17]. Characterization of the SF position can be used to identify how changes to casting parameters influence the quality of the cast product, such as the inclusion of voids within the cast rod, the consistency of the microstructure and the maximum casting rate available for the setup [4].

The physical phenomena underlying the VUCC process can be quantified from CFD simulations but a comparative CFD study into VUCC of OFCu with pushback and dwell applied is lacking. The finite volume Multiphysics software Ansys Fluent^{TM} offers insight into the different thermo/fluidic behaviors and is commonly used to investigate casting phenomena [18].

During solidification, an air gap forms of size approximately 0.1 mm, between the cast OFCu rod and the inner die-mould, which is formed mainly due to the 4.92% volume shrinkage of the OFCu rod on solidification [19]. The formation of an air gap influences heat distribution within the die during solidification [20] as well as other systems, such as phase change materials for energy storage [21,22]. The convective heat transfer coefficient (h_c) is especially an important property characterizing the heat extracted during solidification. Characterizing h_c is crucial for improving the accuracy of CFD modelling, as highlighted in studies into vertically cast Al showing how the air gap altered values for h_c within the die [20,23]. This paper shall aim to characterize how the presence of the air gap and position within the die influences the value for h_c for VUCC OFCu, in order to improve the quality of the CFD model [18].

Three simulations shall be performed with Ansys Fluent^{TM} to study solidification during VUCC of OFCu 8 mm diameter rod. The first, a focused study into the heat transport behaviour within the casting die accounting for the effects of air gap formation to evaluate h_c; the second, inputting evaluated TCR values to simulate solidification behaviour within the entire casting rig; and the third, a focused study of the heat transfer within the casting die, using data obtained in simulation two as boundary conditions for simulation one, to evaluate the influence of die position on heat transfer and h_c.

Simulations were made of VUCC 8 mm OFCu by the company Outokumpu Plc [4], along with measurements of temperature, using a casting setup comparable to the casting conditions applied within this work. The settings applied for their work shall be input to the second simulation, to identify changes in temperature and SF between the two CFD models, and a comparison with their measured temperatures and the developed simulation model shall be used for validation.

The CFD model within this paper shall be compared with castings of OFCu formed by pushback and dwell settings, to further validate the simulation and to identify the phenomena influencing casting quality, such as the position of the SF and microstructure. The fluid flow behaviour within the crucible and die shall be modelled to highlight differences in flow magnitude between these two regions.

The number of articles reporting on VUCC OFCu is limited and so this article shall provide insight into the heat transport phenomena such as, the inclusion of the air gap on the transport of heat from the solidified rod into the graphite die and the application of casting technique ‘pushback’ on the maximum casting speed attainable.

2. Experimental

2.1. Casting setup

8 mm diameter OFCu was VUCC cast under speed settings pushback and dwell, see Table 1 and Fig. 1, to identify the cast grain structure in different orientations of the rod. The speed setting applies a combination of different casting motions within a certain period of time, defined in this study as the casting pulse cycle. The casting was performed in a VUCC machine at the manufacturers Rautomead Ltd, Dundee, UK, and a length of rod was sampled for analysis. Analysis included grinding and polishing to conditions outlined within [24]. The grain structure was then imaged under a high-resolution optical microscope (Spectrographic, NMM-800RF). Columnar grain size was measured on the cast alloy using the software ImageJ.

2.2. Simulation setup

2.2.1. Shear stress transport (SST) k-ω model

Ansys Fluent^{TM} v.R1 was chosen to simultaneously solve solidification, fluid flow and heat transfer. A Reynolds Averaged Navier-Stokes (RANS) flow setting was chosen of k-ω shear stress transport (SST) [25], which was ran alongside solidification to account for the turbulent flow conditions occurring within the crucible melt [10] and the heat transport across the die wall. k-ω SST is shown to be more accurate at modelling near wall interactions in relation to other RANS flow settings [26], and provides a higher accuracy of heat transport phenomena [27]. These factors are useful in the following study for the modelling of the fluid flow and the transport of heat within the casting die. The application of k-ω SST turbulent flow model will highlight the influence, if any, of the turbulent crucible melt flow on the melt flow within the casting die, and the solidification occurring within the die. Additionally, k-ω SST is widely applied for casting modelling [26] and efficiently captures solidification casting flow phenomena without requiring extensive computational time [28]. For details regarding the calculation of the k-ω model see supplemental information.

2.2.2. Enthalpy porosity technique settings

The Enthalpy Porosity technique is applied in Ansys Fluent for the modelling of solidification phenomena. With this technique the melt interface is not explicitly tracked and instead a liquid fraction is applied which indicates the fraction of cell volume in liquid form. The liquid fraction is computed at each iteration based on an enthalpy balance. Over the region of solidification a ‘mushy zone’ region is defined which lies between 0 and 1 within the liquid fraction [29].

For details regarding the equations evaluated see supplemental information.

2.2.3. Computational mesh and solution methodology

Two, 2-D casting simulation models were set up in Ansys as outlined in Fig. 2 and Fig. 3, respectively and three simulations were ran (see Table 2). For details regarding the selected boundary conditions, material parameters and mesh optimization see supplemental information.

The first simulation (simulation model 1 in Fig. 2), investigated the interior of the die and the influence of an air gap on the distribution of heat during solidification from the OFCu, across the air gap and through the graphite die insert. The transient simulation modelled one side of the 8 mm casting die/OFCu (see Fig. 1), setup with a 2D axisymmetry boundary condition. The simulation modelled the condition whereby the OFCu had undergone solidification and was being cast vertically upwards with an air gap formed

Table 1
Casting speed settings.

Speed setting	Total pulse duration (sec)	Upwards (sec)	Dwell (sec)	Pushback (sec)	Average upwards velocity (m/s)	Casting Rate (kg/h)
Pushback (cast)	0.078	0.045	0.021	0.012	0.06	97
Dwell (pause) (cast)	0.369	0.068	0.301	N/A	0.05	80
Continuous upwards motion	N/A	N/A	N/A	N/A	0.022	36
(not cast)	N/A	N/A	N/A	N/A	0.015	24
	N/A	N/A	N/A	N/A	0.008	13

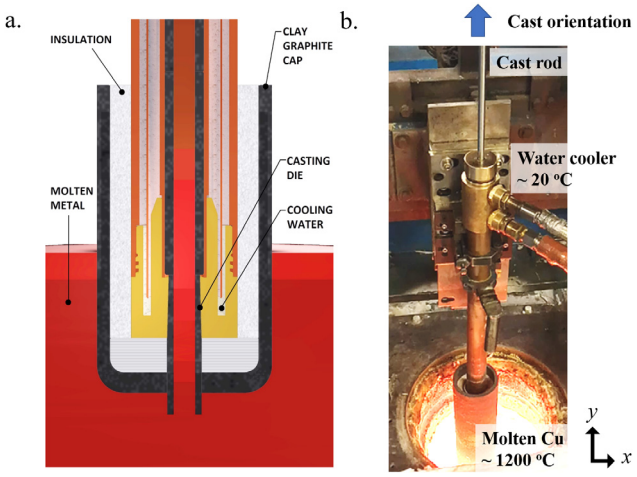

Fig. 1. a) Schematic of the vertically upwards continuous casting (VUCC) 8 mm process. b) Photograph of setup.

between the rod and the die [20]. For this reason, the temperature boundary conditions at the edges of the simulation were set as 20 °C and 1076 °C, on the left- and the inlet/outlet boundaries, respectively, representing the die and cast rod. These temperatures were applied as the left (20 °C), represents the water super-cooler and the inlet/outlet boundaries (1076 °C) a temperature just below its freezing point of OFCu. When solidified, the OFCu undergoes shrinkage forming the 0.1 mm air gap [20] and so, modelling OFCu in the solidified state rather than the liquid better captures the real casting conditions.

The simulated domain was set up with a quadratic, structured mesh and a mesh convergence study was performed for the different sizes of total cell numbers 21,050; 42,100; 84,200; 168,000; and 336,800. The convergence criteria were continuity 10^{-3}; velocity components in x- and y-directions, k (turbulent kinetic energy) and ω (dissipation rate) as 10^{-4}; and energy as 10^{-6}. The convective heat transfer coefficient within the Cu melt domain was evaluated without an airgap (see section 2.3) for the different mesh sizes (cell numbers) see 2b. This shows that for the cell count 84,200, little change occurs with the measured convective heat transfer coefficient for greater cell numbers. The Grid Convergence Index (GCI) was evaluated for the different mesh numbers, (see supplemental). It was identified that the 84,200 cell size displayed an extremely low GCI value of ± 1.1 W/m^2K highlighting that the solution was resolved and that further grid refinements were not needed.

With mesh optimization for simulation model 1, it was ran with and without the inclusion of the air gap, and the TCR was evaluated (see section 2.3) across the Die/OFCu.

Simulation model 2, modelled the entire casting crucible, including the graphite die inset as shown in Fig. 3a) & b). Heat was supplied at 20 °C and 1200 °C by the super cooler and the heat inlets, respectively. The heat inlets represent the resistant heaters used in VUCC. The top of the crucible was set to an 'outflow' boundary condition (an Ansys specific annotation – see supplemental for complete description), who's velocity is evaluated within the software based on the velocity set at the 'outlet' boundary (see Fig. 3b). This setup represents a full casting rig being continuously resupplied with copper feedstock. The top of the die was set to a 'velocity outlet' boundary and to cast upwards at a rate determined by the relevant speed setting to be applied, see Table 1. To improve accuracy of the simulation, Marangoni forces generated, due to changes of the OFCu melt viscosity because of changes to temperature [27], were applied to the inner die wall boundary condition, using the value for copper surface tension temperature gradient of -0.425×10^{-3} N/m. K, reported in [28]. All other boundary conditions were set to a 'wall' condition. Other simulation parameters applied include running with a pressure-based solver; an absolute velocity formulation; a gravity operating condition of -9.81 m/s^2 in the y-axis; and a coupled pressure–velocity coupling scheme.

The simulated area was set up with a hybrid, quadratic/triangular mesh. Mesh optimisation of this setup was performed by the group within [16] and optimal conditions were evaluated as sizes 2×10^{-3} m, 1×10^{-3} m and 1×10^{-4} m for: the main crucible; within the die insert/ super-cooler/ cladding/ cap; and the OFCu within the die, respectively, as highlighted in Fig. 3. The cell size was reduced in areas of small features and kept large in others to reduce the overall simulation time, for a total cell count of 305,796. The different materials simulated here included: the cap and crucible wall set as graphite; the super-cooler and melt set as copper (as super-coolers are made from copper alloy); and the cladding material (calcium-manganese silicate, supplied by RS under 724-8906) used in the casting rig. The simulation conditions for these materials is highlighted in the supplemental information. Time step size was selected based on an adaptive time-stepping method (see supplemental information for details).

Simulation 3, applied to model 1 (see Fig. 2) introduced different heat inlet boundary values from three positions within the die, obtained from the simulated results for simulation 2. Details of this setup are provided in the supplemental information.

Highlighted in Table 2 are different casting speeds applied within the simulation which include pushback setting, dwell setting and casting at one speed continuously. to apply these settings a transient simulation was chosen and measurements taken once the simulation reached a state of equilibrium. Simulation equilibrium was determined by evaluating the conditions for a continuous temperature and solidification output for the periodic transient setting applied (see Table 1), and the conditions for convergence were the same as for simulation model 1. The 0.022 m/s continuous speed settings applied, see Table 1, represents the maximum speed setting for the similar, upcast ofcu process, reported within [4]. other speed settings reported in their work were simulated and the measured thermal profiles produced within the die for those speeds were compared for validation of the simulation modeled in Table 2 are different casting speeds applied within the simulation which include pushback setting, dwell setting and casting at one speed continuously. To apply these settings a transient simulation was chosen and measurements taken once the

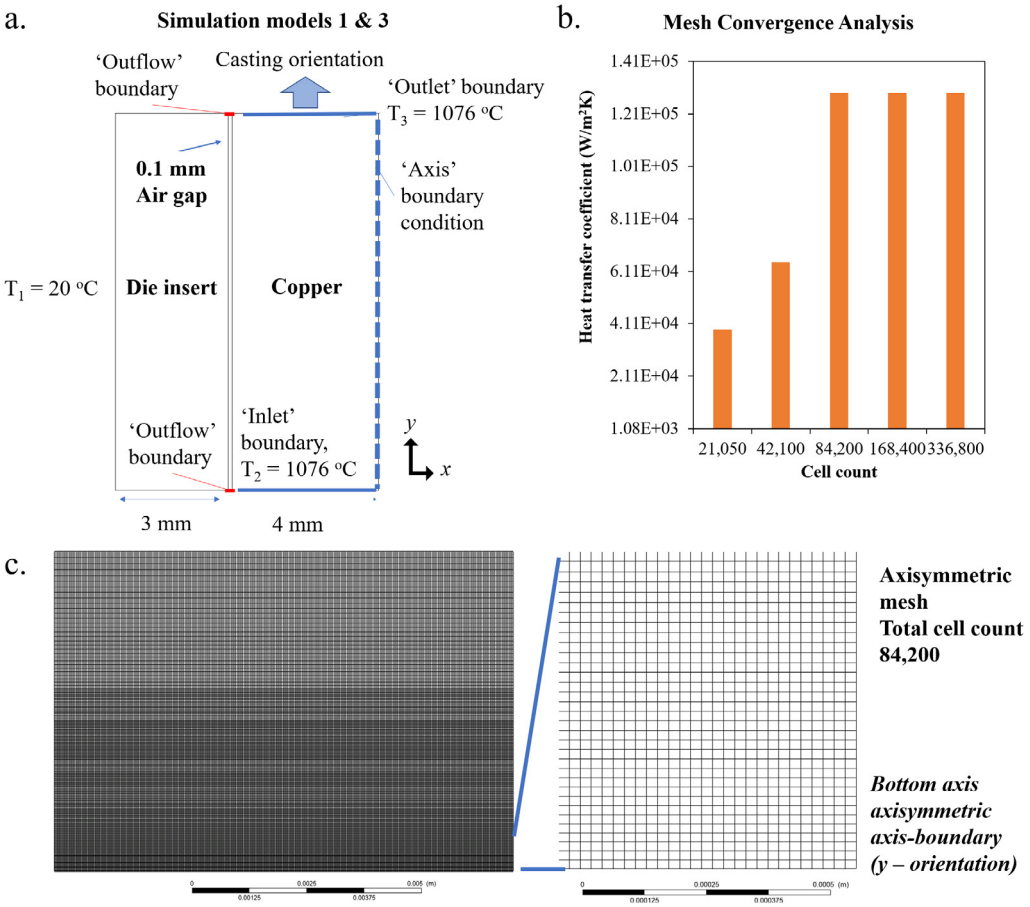

Fig. 2. a) Schematic of 2-D axisymmetric simulation setup for simulation model 1 & 3 of air gap within the die and b) mesh optimization without airgap. c) The optimal mesh size.

simulation reached a state of equilibrium. Simulation equilibrium was determined by evaluating the conditions for a continuous temperature and solidification output for the periodic transient setting applied (see Table 1), and the conditions for convergence were the same as for simulation model 1. The 0.022 m/s continuous speed settings applied, see Table 1, represents the maximum speed setting for the similar, Upcast OFCu process, reported within [4]. Other speed settings reported in their work were simulated and the measured thermal profiles produced within the die for those speeds were compared for validation of the simulation model.

2.3. Evaluation of heat transfer coefficient.

The software Ansys Fluent™ can output the convective heat transfer coefficient (h_c) (W/m^{2}K) at the die wall, which is given by:

$$h_c = q_h/(T_s - T_{ref}) \quad (1)$$

where q_h is the heat flux, T_s is the temperature of the graphite die wall and T_{ref} is the temperature of the liquid medium close to the wall, which in this case is the air gap, or the liquid metal if the air gap is not included [30].

From this, the thermal contact resistance (TCR) (m^{2}K/W) [18] is evaluated as:

$$TCR = 1/h_c \quad (2)$$

The value for TCR evaluated in simulation 1 was input into the boundary conditions of the inner wall within simulation 2, as highlighted in Fig. 2b.

2.4. Design of experiment

A series of simulation investigations were performed as outlined within Table 2.

3. Results and analysis

3.1. Air gap modelling

The inclusion of an air gap between the cast rod and the graphite die wall was investigated from CFD simulations and the solidification and thermal effects studied. Highlighted in Fig. 4 is the simulated heat distribution across the solidified OFCu and the graphite die. Shown in Fig. 4a is the heat distribution for the solidified OFCu with the air gap removed from the simulation (set as a graphite material). The simulation shows the outcome for solidification of the OFCu using VUCC with the pushback setting, whose average orientation is highlighted by the two arrows. The result shows how heat is transported from its introduction at the inlet of the simulation, which is set at 1076 °C and represents the heat within the rod after solidification, to the left-hand side - which is set at 20 °C and represents the influence of the super cooler. The width of the graphite die is to scale and shows that heat is transferred from the OFCu into it.

Highlighted in Fig. 4b is the distribution for the same area and setup, but with the air gap changed to an air domain. Here the heat transferred from the solidified OFCu to the graphite die is considerably less than without the air gap, as indicated by the higher and lower temperatures within the melt and die, respectively.

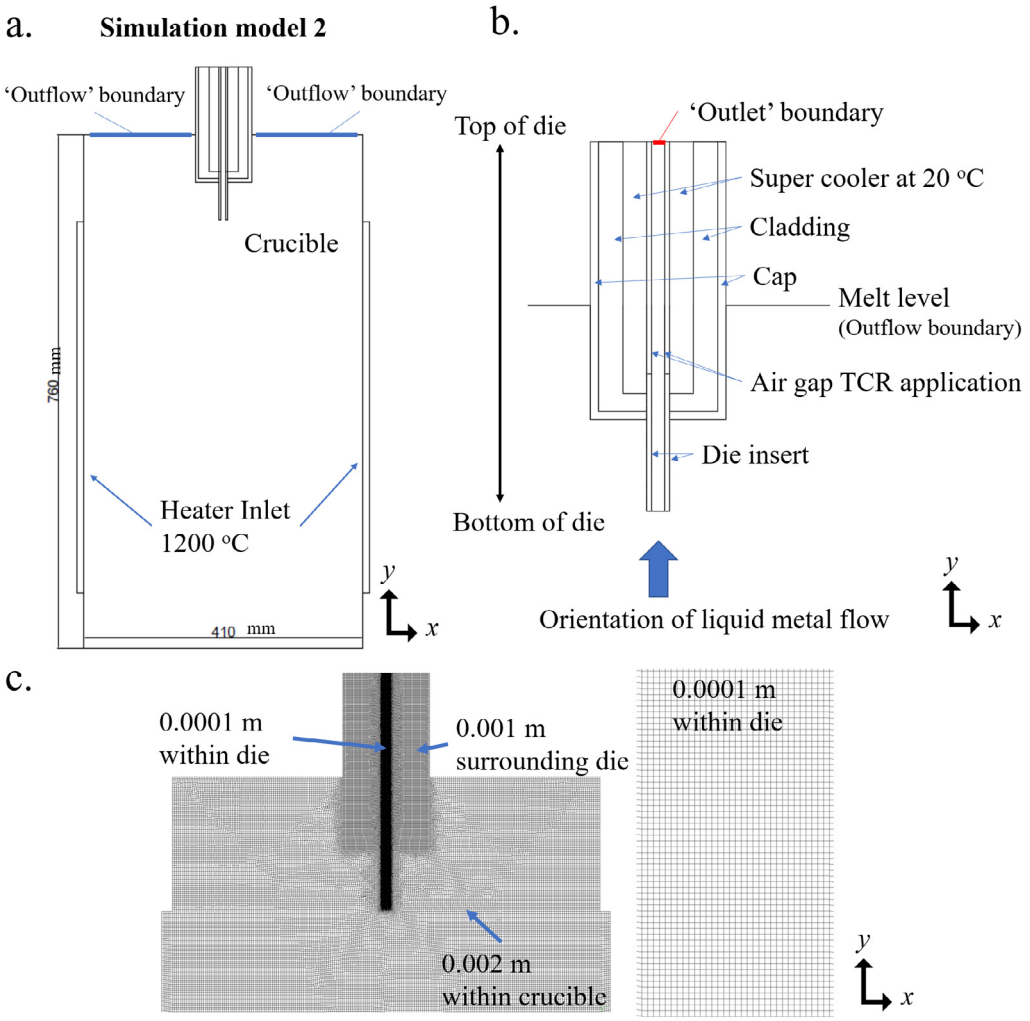

Fig. 3. Schematic of Simulation model 2, showing a) & b), the crucible and a close-up of the die region, respectively and c) the generated optimal mesh showing close-up within die.

Table 2
Simulations performed.

Simulation number	Settings altered	Purpose
1	Set the air gap domain to a graphite material	To identify heat transport without air–gap
	Set the air gap domain as air material	To identify the heat transport with air–gap inclusion
2	Set the Cu movement out of the simulation to pushback and dwell settings	To identify CFD behaviour for standard VUCC conditions for 8 mm diameter OFCu
	Set the Cu movement to 0.022 m/s, 0.015 m/s and 0.008 m/s continuous	To identify how CFD behaviours alter with previous work in the research field and validate simulation model
3	Boundary conditions, inputting values output from simulation 2 into simulation 1.	Model the change of h_c in relation to vertical die position.

The air gap shows a thermal conductivity of approximately 0.077 W/m.K [31] which is significantly lower than the thermal conductivity of the solidified OFCu and the graphite die, at 157 W/m.K [32] and 53 W/m.K, respectively. As such, the air is found to act as a barrier to the transport of heat.

Highlighted in Fig. 4c is the horizontal temperature distribution taken from across the simulation for the two different settings. At position 2.9 mm around the interface of the die and the OFCu, the temperature gradient is considerably greater for the inclusion of an air gap, which hinders the transport of heat from the solidified OFCu into the die. This simulated outcome represents more realistic conditions for casting once the rod is solidified, as demonstrated by the similar temperature distribution measured off horizontally cast copper in [33]. Additionally, the simulation includes approximation for the formation of a 0.1 mm air gap between the solidified OFCu and the casting die - which forms during casting conditions due to shrinkage of the solidified metal as demonstrated in [34] and [4]. The net effect of the air gap on solidification is to retain a greater amount of heat within the OFCu rod, which is observed in other vertical casting setups such as with aluminium [20].

The average convective heat transfer coefficient (h_c) was evaluated vertically across the OFCu / die interface for with and without the presence of an air gap and reported in Fig. 4d as $(9.0 \pm 0.2) \times 10^4$ W/m^{2}K and $(1.3 \pm 0.1) \times 10^5$ W/m^{2}K, respectively. Values for h_c evaluated from literature simulations of OFCu horizontal slab casting [33] and from measurements of copper cooled in water [35], were $(0.955–1.896) \times 10^3$ W/m^{2}K [33] and $(0.13–1.2) \times 10^4$ W/m^{2}K [35], respectively. The values obtained in this work are comparable to literature values, where differences occurring are

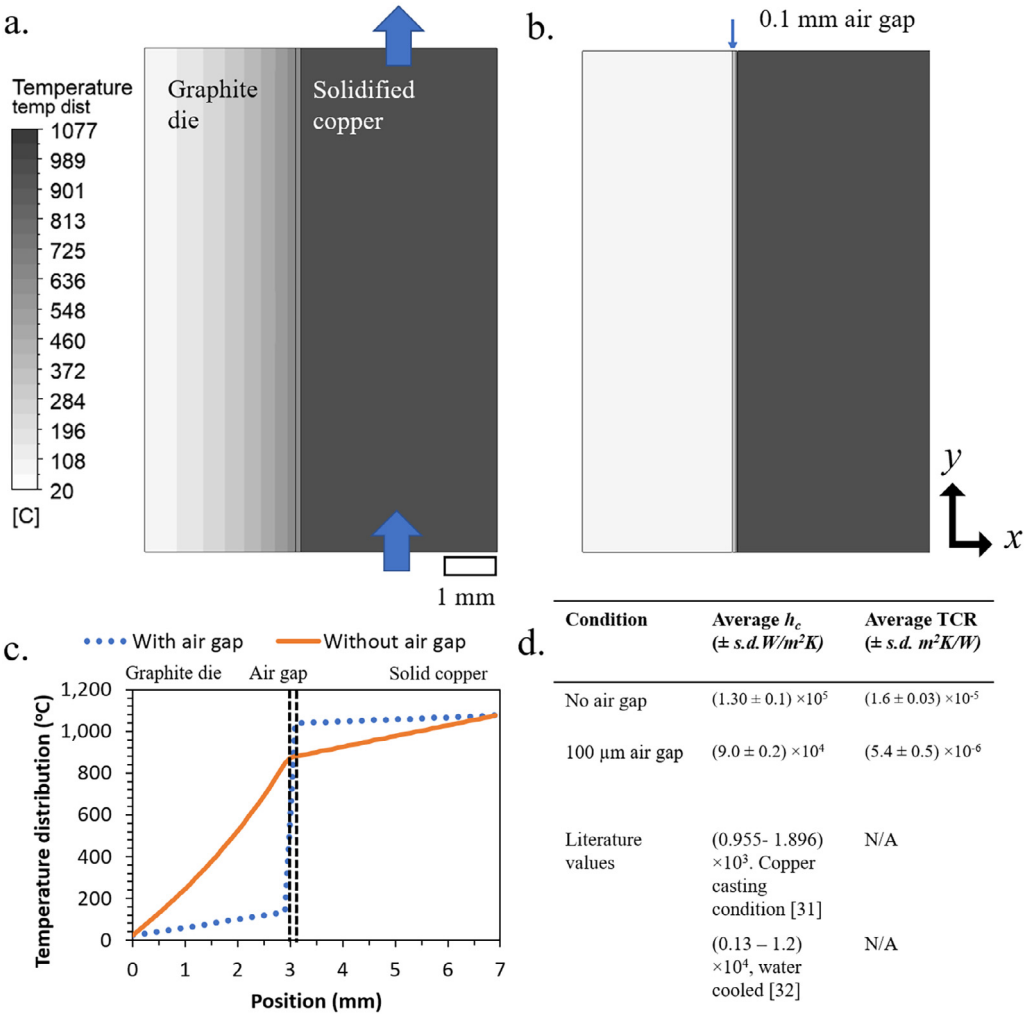

Condition	Average h_c (± *s.d.W/m²K)*	Average TCR (± *s.d. m²K/W)*
No air gap	(1.30 ± 0.1) ×10⁵	(1.6 ± 0.03) ×10⁻⁵
100 µm air gap	(9.0 ± 0.2) ×10⁴	(5.4 ± 0.5) ×10⁻⁶
Literature values	(0.955- 1.896) ×10³. Copper casting condition [31]	N/A
	(0.13 – 1.2) ×10⁴, water cooled [32]	N/A

Fig. 4. Simulation of solidified OFCu metal/graphite die interface, showing with arrows the orientation of the average pushback casting movement and the temperature distributions for A) without air gap and B) with 0.1 mm air gap. C) Horizontal temperature distribution across simulation showing with dashed lines position of air gap. D) Table insert of measured values.

likely due to differences with casting properties such as velocity and geometry, and the temperature of the cooled metal.

Without any air gap the setup assures perfect contact of the cast metal and the die wall, and the transport of heat into the die is considerably larger, as demonstrated by the order of magnitude higher h_c value obtained in this study. However, this setup is unrepresentative of VUCC of copper alloys [36] and, for this reason, the smaller h_c value evaluated for the inclusion of the air gap shall be converted to TCR and input into the boundary conditions of the inner die wall, see Fig. 2c, for large-scale solidification studies of the casting rig, disseminated in sections 3.2–3.5.

3.2. Heat influence on casting

Highlighted in Fig. 5 are 2-D images of the thermal distribution within the casting setup, showing in a) & b) the entire casting area and a close up of the die, respectively, for casting with pushback setting. Hot regions of approximately 1200 °C are highlighted in dark and the coldest regions, at above 20 °C, by white. The thermal equilibrium conditions are displayed and show that, as the OFCu is cast upwards, heat is dissipated starting from the edges of the die. Most thermal changes occur within the die rather than within the crucible, which is due to the cooling of the melt as it enters and is influenced by the super-cooler's temperature.

After the onset of contact with the super-cooler and up to position *b.* (Fig. 5b), the temperature distribution in the middle of the die-melt displays a concave shape of high temperature surrounded by a lower temperature sheath. The high temperature region is likely due to re-heating of the OFCu after solidification, due to latent heat given out by the solidification process [37], and heat which is yet to be extracted as the OFCu is cast upward. After position *b.* which is at around 150 mm vertically along the die, the high temperature feature tapers and the values in the die middle and at the walls drop, tending toward a more uniform temperature distribution across the die, as also shown in Fig. 6a.

Highlighted in Fig. 5c is the temperature distribution for the casting speed setting continuous upwards at 0.022 m/s. With this slower speed the heat within the die is smaller and is distributed lower down around the onset of contact with the super-cooler, indicated by position *c.* This setting was also applied in [4], and highlighted a similar size and shape of the thermal distribution.

The influence of the temperature distribution reported was investigated in relation to changes to h_c evaluated at the interface between the OFCu – airgap-graphite die wall (see section B in supplemental). Using simulation model 1 with boundary conditions applied using values obtained from Fig. 5b, h_c was evaluated from three positions in the die, from around the onset of solidification at the super cooler (position a. in Fig. 5b) to higher up within the die,

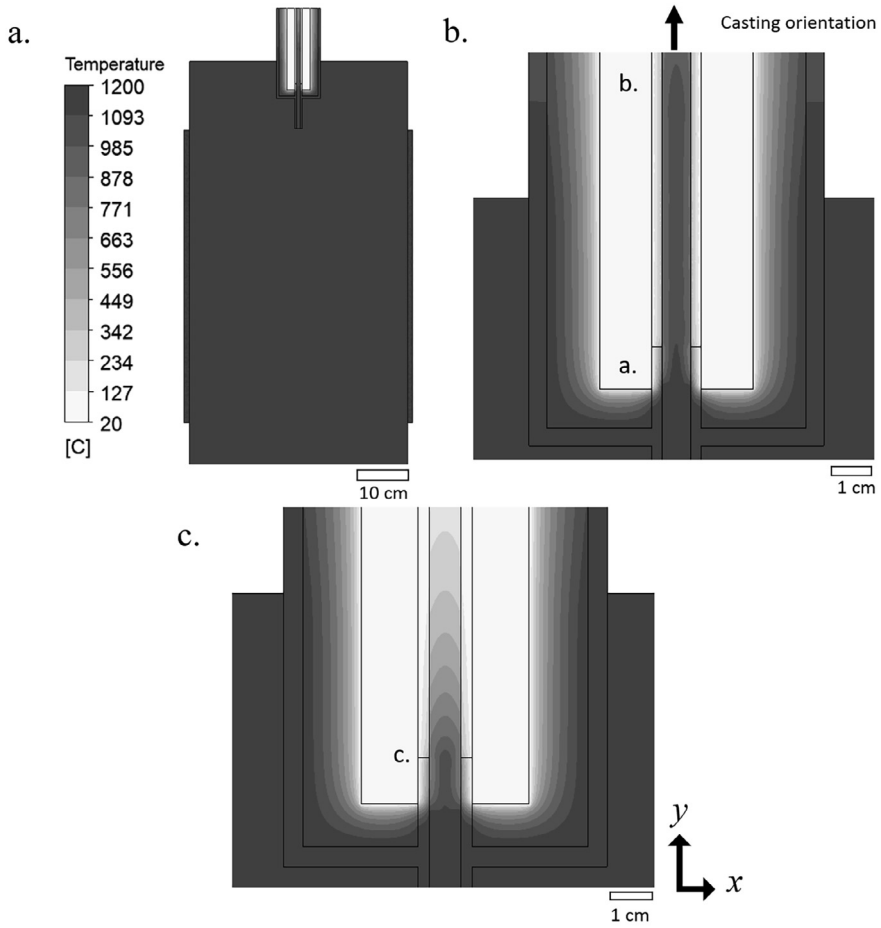

Fig. 5. 2-D simulated casting for OFCu metal, showing thermal distribution (dark = 1200 °C, light = 20 °C) for pushback setting (0.06 m/s average), over A) the entire simulation, B) within the die and C) upwards motion casting setting (0.022 m/s) within the die.

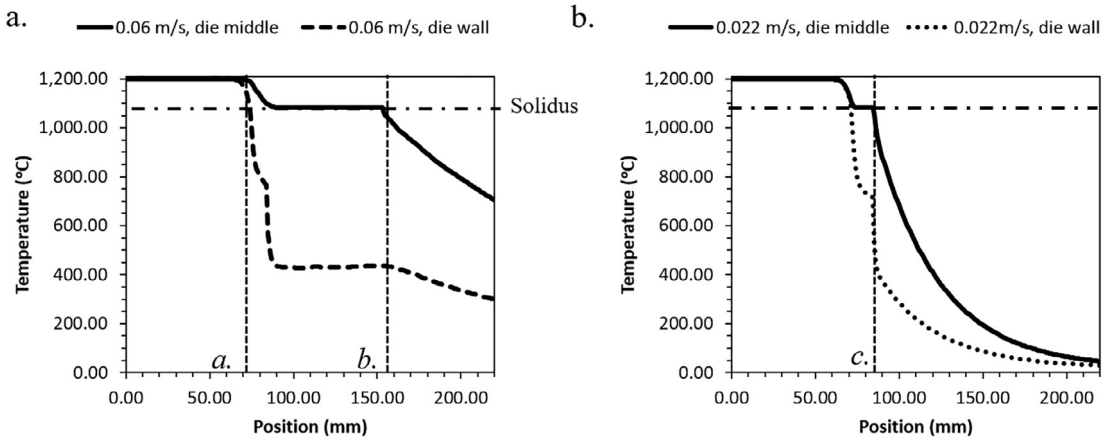

Fig. 6. Simulated plots of the thermal distribution from die bottom to top (along y axis) for casting settings a) pushback (0.06 m/s average) and b) continuous at 0.022 m/s, respectively.

(position b. in Fig. 5b). h_c measured from simulation reduced from $(5.99 \pm 1) \times 10^5$ W/m^{2}K to $(2.47 \pm 1) \times 10^3$ W/m^{2}K. Further up in the die h_c reduced further to negligible values of $(1.5 \pm 0.1) \times 10^{-10}$. This high variation was attributed to the reduction of heat from the rod as it was cast upwards and the resultant changes in heat flux in those regions, $(1.85 \pm 0.4) \times 10^7$, $(8.70 \pm 3) \times 10^5$ and $(4.71 \pm 3) \times 10^{-8}$, accordingly. The results highlight that h_c across the OFCu–airgap-graphite die wall will vary locally as the OFCu is cast upwards and cools, which is in line with findings observed with vertically cast aluminium [20,23].

Highlighted in Fig. 6a, is a plot of the thermal distribution from along the inner die wall, vertically from its bottom to top, at the interface with the OFCu melt and along the center line of the die. The solidification temperature (solidus) is highlighted by the

horizontal dashed line at 1084 °C. The position of the super-cooler onset along the die is marked by *a.* see Fig. 5b, which is highlighted on the plot by a vertical dashed line around 70 mm along the die.

The temperature across the OFCu in the die varies with greater values in the middle. This behaviour is due to colder temperatures occurring at the die-wall interface, due to the higher cooling rates within these regions relative to the slower rates and hotter temperatures observed in the center of OFCu rod, which is in line with continuous casting behaviour [4]. At position *a.*, the OFCu is first cooled down and as it moves upwards, and cools to approximately 430 °C and 1080 °C, at the die wall and middle, respectively. These temperatures are below and around the freezing point of copper (1083 °C), accordingly [38]. From die position 70–150 mm (positions *a.* to *b.*), the temperatures plateau at both the middle of the die and at the wall, before dropping off after 150 mm (position *b.*). The length of this plateau is approximately 60 mm for the pushback simulation settings. The heat generated here is due to a), convection from the melt as the OFCu is cast upwards and b), the latent heat of solidification produced due to OFCu transition from liquid to solid [36]. The consistent temperature over this region is a solidification phenomena occurring with metals, whereby the temperature of a system remains constant until all of the material is solidified, due to the heat given out during solidification being balanced by the latent heat of fusion generated in forming the solid state [39]. The casting setup in the simulation is a dynamic system with the OFCu being cast upwards and so the heat within the centre of the die is high after the onset of solidification at position *a.*, and is constant until solidification is complete around position *b.* The temperature profile produced provides a rough indicator as to where solidification occurs within the die, as confirmed in section 3.3.

At position *a.,* the temperature at the wall of the die drops due to heat extracted across the die. This is shown in Fig. 6a as temperature drops of approximately 1200 °C to 800 °C, followed by a further drop of 800 °C to 400 °C. The second drop is due to the low h_c which in turn is due to the air gap hindering the transport of heat and further reducing the temperature at the die wall.

After position *b.,* the temperatures drop in the die middle and wall due to dissipation of heat towards the super-cooler. Also, the temperature difference between the two regions becomes smaller, which is in line with casting behaviour [4].

Highlighted in Fig. 6b is the temperature plot for the casting speed setting 0.022 m/s upwards only. As with the faster speed of 0.06 m/s, the temperature is less at the die wall than the centre, although the temperature plateau is less pronounced finishing around 84 mm, noted by the vertical dashed line and point *c,* see Fig. 5c. For faster speeds the solidification finished around *b.* and for the slower speeds it finished around *c.,* as confirmed in section 3.3. This is likely due to the slower casting speed enabling the heat to be transported out of the die sooner as it is cast upwards, resulting in solidification occurring quicker within the die and at a position lower down, producing a smaller average temperature within the die.

The temperature distribution vertically within a 8 mm VUCC OFCu casting die was measured by Härkki K and Miettinen J in [4] and the values obtained plotted in Fig. 7a, showing the measured temperature profile for three different casting speeds (0.022 m/s, 0.015 m/s and 0.008 m/s), between positions *a.* and *b.* The die region was specified within [4] in terms of % of a position between the supercooler and further up within the die after solidification. The measured temperatures were between 50 °C and 160 °C with higher temperatures occurring around the onset of the super cooler (position *a.*) and reducing along the inside of the die as the rod is drawn outwards (position *b.*). The temperatures within the die (50 °C–160 °C) are less than those on the inner die wall (1200 °C–400 °C, Fig. 6a&b), due to thermal conduction over

a.

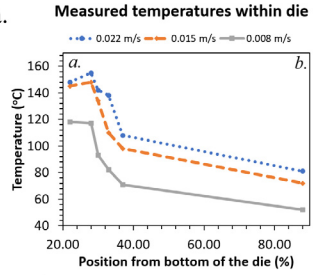

b.

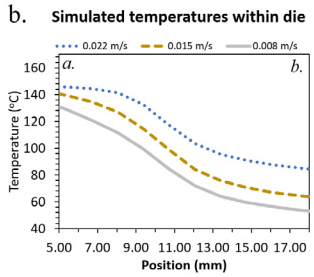

c.

		Cast speed		
		0.008 m/s	0.015 m/s	0.022 m/s
Position a. (5 mm)	Measured Temperature (°C)	118	145	148
	Simulated Temperature (°C)	129	139	146
Position b. (19 mm)	Measured Temperature (°C)	52	72	81
	Simulated Temperature (°C)	52	62	83

Fig. 7. a) Measured thermal profile inside the graphite die vertically for different casting speeds from [4]. b) Simulated plot of temperature inside graphite vertically for different casting speeds. c) Temperature comparisons between measured and simulated thermal values.

the air gap, see section 3.1. For faster casting speeds greater temperatures were measured within the die attributed to the slower rates of heat loss over the cast duration, confirming the simulated results within Fig. 6.

To validate simulation model 2 it was ran with three continuous withdraw speeds (0.022 m/s, 0.015 m/s and 0.008 m/s) and the temperature distributions were extracted from inside the die vertically between positions *a.* and *b.* The simulated temperature profile in Fig. 7b highlights a similar trend for the heat distribution, as the simulated values occurring around position *a.* at 5 mm and position b. at 18 mm, were to within 11 °C of measured values, see Fig. 7c.

3.3. SF position during casting

Highlighted in Fig. 8a and b are distributions of OFCu solidification within the die, showing in grey the solidified metal for casting speed settings pushback (0.06 m/s, average), and 0.022 m/s continuous, respectively. The interface between the liquid melt and the frozen metal is the SF highlighted in black. Also shown is the outline of the other components in the die, although they are not included in the solidification display. Solidification starts at the die wall near to the super-cooler, marked by the lower arrow, because of the lower temperatures in this region and is observed to start here in other CFD simulation models [4]. The centre of the die is the hottest region and so remains a liquid for longer as the OFCu is cast upwards, giving the SF a sharp peak appearance. This shape is influenced by the orientation of the rod as it is cast, such that in vertical downwards casting a pointed SF is also produced, but facing downwards [40]. In pure metals solidification occurs over a finite range as controlled by the temperature gradient within the die, unlike metal alloys where the SF is more gradually dispersed between liquidus and solidus regions, due to differences in melting temperature between the different metals [39]. As such, the liquidus to solidus region occurs over a finite well-defined interface within the OFCu rod.

For slower speeds the shape of the SF is characterised by a smaller extension up the middle of the die, as shown in Fig. 8b. This is

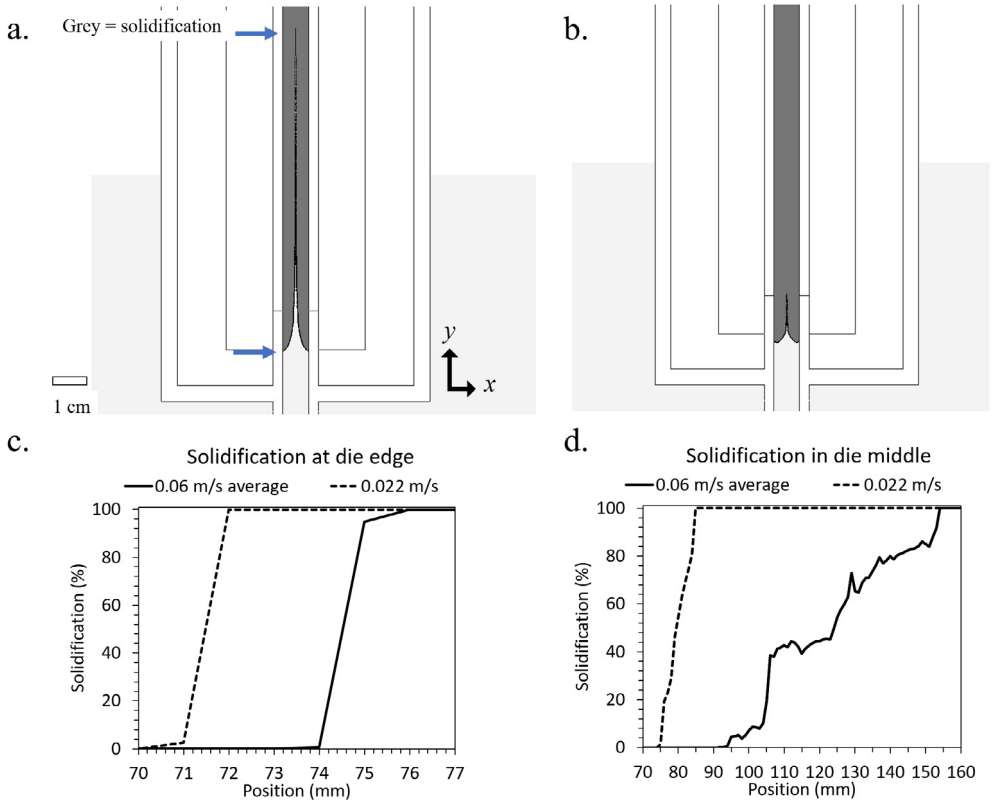

Fig. 8. 2-D simulated casting for OFCu metal showing mass fraction of solidification for a) pushback (0.06 m/s average), and b) continuous motion (0.022 m/s). Plots of the mass fraction vertically along the die wall (along y axis), at positions c) at the die wall around super cooler and d) in the middle of the die between the two blue arrows.

due to the smaller temperature gradients generated within the melt at slower speeds, see Fig. 5, enabling solidification to complete lower down within the die centre.

Highlighted in Fig. 8c is a 2-D plot of simulated solidification for pushback (0.06 m/s average) and 0.022 m/s, along the inner wall of the die vertically, taken at a position around the lower arrow in Fig. 8a. Displayed is the percentage mass fraction for solidified OFCu within the melt, as the mass of a species per unit mass of the mixture. Solidification begins for both casting speeds around the same location to within 4 mm, indicating that for the casting speeds applied the influence on SF position does not alter significantly.

Highlighted in Fig. 8d, is the percentage of solidified OFCu at the die middle, vertically between the two arrows, noted in Fig. 8a. For both speeds over this region the solidified OFCu increases until it is completely solidified. The centre of the die remains liquid for longer compared to the die wall, as indicated by the higher degree of solidification at the wall. These lengths are 60 mm and 10 mm for casting speeds pushback (0.06 m/s, average) and 0.022 m/s, respectively. The region is significantly longer for faster casting speeds due to the lower heat extraction as noted in section 3.2.

For the faster speed (pushback, 0.06 m/s), as the OFCu is cast upwards in the die, solidification increases, but also decreases temporarily as noted around positions 115 mm and 132 mm, before increasing again. These localised reductions in solidification are likely due to random convective motions of the liquid melt within the die altering the temperatures and lowering the degree of solidification [36].

The faster casting speed is desirable as it enables increased throughput of the cast rod, however, increasing the casting speed leads to casting defects such as cavity shrinkage and gas porosity [41], resulting in a reduction to the cast mechanical properties as demonstrated in the casting work by [42], [5] and [43]. In the VUCC of 8 mm OFCu with pushback, the speed is limited to an average of 0.06 m/s or 139 kg/hr, after which defects start to occur. For increased casting speeds it is predicted that the SF will extend up within the die, which follows the trend noted here and in [4]. The formation of unwanted voids or hollow rods is possibly due to this effect and so, for casting speeds beyond 0.06 m/s average, the temperature within the rod is likely to be too great for the VUCC setup modelled. The publishing of maximum cast speeds is typically not discussed in literature due to variations between casting setups and applied alloys influencing this value, but the previous maximum reported speeds for 8 mm upcast, OFCu in the Outokumpu process is 0.022 m/s [4]. This value did not include the application of pushback and so was likely limited due to this.

3.4. Pushback and dwell on cast grain structure

Highlighted in Fig. 9 are measured optical images of the longitudinal (rectangular) cross sections, of a VUCC 8 mm OFCu rod, with simulated SF contours plotted over the surface, for a) pushback setting 0.06 m/s average and b) & c) dwell setting 0.05 m/s average. The rods have been etched and the grains are revealed, showing grain structure characteristic of OFCu casting, which are small grains within the centre, columnar grains between the centre and edge, and equiaxed grains on the outer edges, referred to as the 'chill zone' [44]. A symmetry is displayed in the growth of the grains around the rod centre. When casting, if the SF is significantly asymmetrical relative to the centre, then VUCC is applied with pushback or dwell for 8 mm rods, the SF is likely symmetrical within the rod as demonstrated in the simulated outcome in Fig. 8, but with some slight asymmetry due to random convective

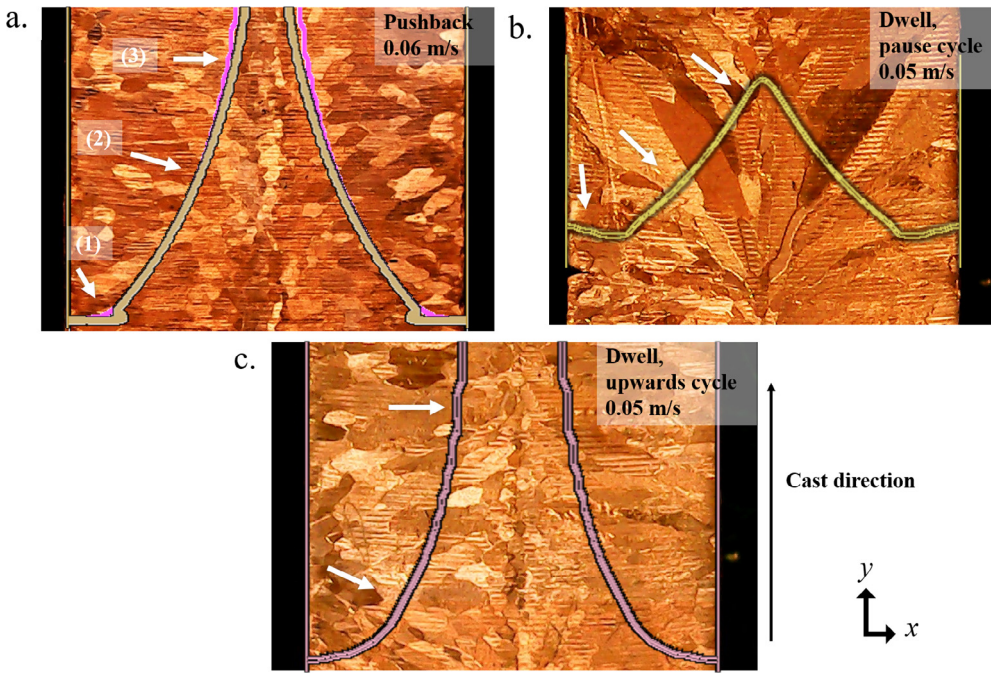

Fig. 9. Longitudinal cross sections of 8 mm diameter rod, showing grain growth direction by white arrows, with simulated SF overlaid, for a) pushback cast sample (0.06 m/s, average), showing SF for upwards and pushback cycles shown as pink (light) and yellow (dark), respectively; and b) & c) dwell setting (0.05 m/s, average) for the pause and upwards movements of the casting cycle, respectively.

currents within the melt and a variation in the vertical alignment of the casting die due to its instillation.

The pushback casting setting is comprised of an upwards and backwards movement. The SF produced for both movement settings has been overlaid in Fig. 9a, showing upwards and pushback by pink (light) and yellow (dark) lines, respectively. For the pushback setting, there is little difference between the orientations of the SF during the casting pulse. In this configuration the grains grow from the edge to the middle of the rod [4], (numbered 1 to 3), and over this region, their orientation shifts from parallel to perpendicular to the casting direction (which is upwards in the figure). The grain growth direction indicates the orientation of the heat extraction from the liquid metal (below the SF) into the solidified metal (above the SF). Metal grains grow from normal to thermal isotherms within a solidifying configuration [44], and so the grain alignment here is also normal to the SF. For the pushback setting, there is little difference between the SF for the different motions in the pulse cycle and so the copper grain orientations also undergo little change due to these motions.

For the dwell setting, in Fig. 9b & c, there is a large change between the upwards and pause motions within the casting cycle. For the application of the pause, the SF protrudes less up the middle of the die which is the same behaviour witnessed for slower casting speeds, see Fig. 8. During the pause cycle of the dwell setting (Fig. 9b), the growth direction of the copper grains alters, characterised by the grain's orientating themselves closer to a parallel alignment to the casting direction. Additionally, the columnar grains show a large average area, (2.4 ± 0.7) mm^2. For the upwards movement of the dwell setting (Fig. 9c), the SF is positioned further up the die and the grain growth direction changes, orienting from the normal to the cast direction. The columnar grains are also of a smaller average area, (0.5 ± 0.2) mm^2 for this configuration. As the motions change within the casting pulse the simulated results can reproduce the casting conditions leading to the observed changes in grain orientation.

For the cast example, the difference in grain size between the two settings is related to the changes in the cooling rate between the two motions. During dwell, the cast rod is held within a hotter region for longer (below the supercoolers), reducing the rate of cooling. Larger grains can form at slower cooling rates [36] and so the larger grains observed within Fig. 9b highlight this behaviour. Larger grains produced within OFCu and copper alloys coincide with weaker yield strengths for the cast rod and are of lower quality for casting applications [5].

The grain structure behaviours witnessed for the two casting movements, pushback and dwell, is also witnessed for large changes to the average casting speed. For 8 mm OFCu cast at slow speeds (below 0.5 m/min) the grains are larger and display a parallel alignment to the casting direction, and for faster speeds (greater than 0.5 m/min) the grains are smaller and perpendicularly aligned, as outlined within [2]. The application of pushback or dwell can locally reorient the grains within a casting pulse cycle, to produce a desirable casting microstructure and properties, with pushback showing a more desirable control for the cast outcome.

The grain structure will also display a growth direction within the rod influenced by this positioning [45]. The results produced here show that when.

3.5. Fluid flow velocity on casting

Highlighted in Fig. 10 are plots of the 2-D distribution of simulated fluid flow and solid motion over the entire simulated area, and a close up of the die region, respectively. The boundary condition at the top of the die was set to the pushback casting setting (see Fig. 3), which comprises of upwards motion followed by a dwell and a pushback. Fig. 10 displays the flow conditions during the upwards portion of the casting cycle only. During this setting, the solid motion occurs within the die where the liquid has undergone solidification around the super cooler, and is drawn out of the simulation at the top boundary of the die.

Indicated by the small arrows in Fig. 10a, is the normalised motion orientation which indicates the fluid flow orientation and the solid motion orientation as the simulation evolves in time. By the large arrow at the top of the simulation, which is the region

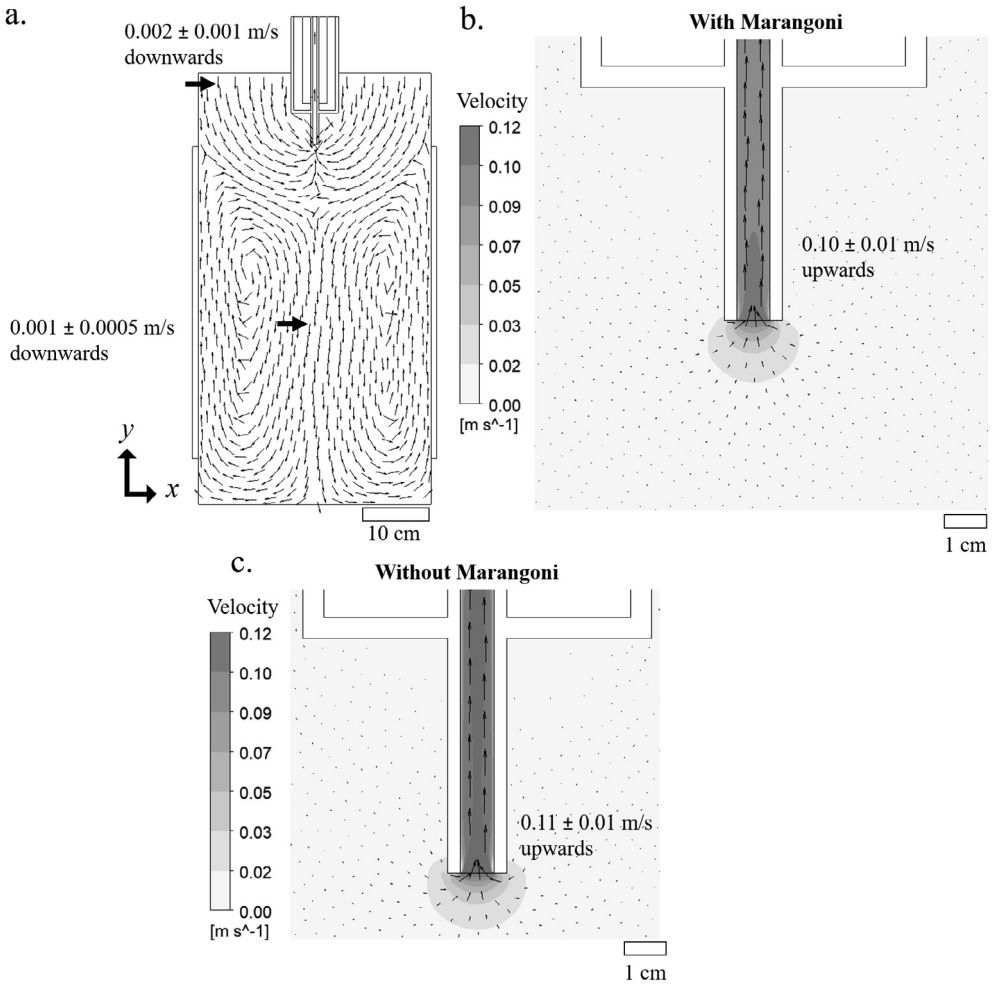

Fig. 10. 2-D simulated casting for OFCu metal (0.06 m/s, pushback), showing copper fluid flow and solid motion. a) Fluid and solid orientations only for the upwards pulse cycle, for the entire crucible, b) the fluid orientation and magnitude within the crucible/die entrance and c) without Marangoni boundary conditions.

by the open boundary condition representing the refilling of the crucible by liquid Cu metal feedstock, the average flow rate is measured as 0.002 ± 0.001 m/s downward. The fluid is next directed towards and through the casting die where the fluid solidifies and exits the simulation by the top of the die. Within the crucible, fluid motions are generated due to natural convection and show a symmetrical distribution with vorticity occurring on either side. At the edges of the crucible fluid flow runs vertically upwards, with a downwards flow (noted by the large arrow), in the centre of the crucible of 0.001 ± 0.0005 m/s. The motions within this region are induced by temperature gradients generated by the heat inlets on the edge of the crucible wall; the casting velocity; and gravity [28]. The thermal distribution within the crucible is low as also shown in Fig. 5, and so, the magnitude of the fluid motion here due to natural convection is low.

Fig. 10b highlights the fluid flow and solid motion within the crucible and die, with the arrows showing orientation and, by their size, velocity magnitude. Included in grey are the velocity magnitude contours. The fluid is drawn into the die from the regions surrounding the die tip and at a rate of 0.10 ± 0.01 m/s upwards and is significantly larger than the flow occurring within the crucible or at the top of the melt. Fluid flow influences solidification and during casting the flow generated within the crucible due to natural convection will likely have little influence on the SF position due to its smaller magnitude. The exiting speed of the solidified copper metal, for the upwards portion of the 'pushback' casting setting (see Table 1) is 0.1 m/s and the flow into the die approximates this exit motion of the solid OFCu.

At the edges of the inner die walls a Marangoni boundary condition was applied, which contributed to the convection and fluid movements generated there [46]. A simulation was ran without Marangoni boundary condition applied, see Fig. 10c. The fluid flow generated due to Marangoni forces did not appear to significantly alter the fluid motions within the die before solidification, as shown by the uniform orientation of the flow arrows up the die and similar average velocity magnitudes across the die of 0.11 ± 0.01 m/s and 0.10 ± 0.01 m/s, for without and with Marangoni convection, respectively. As such, Marangoni convection did not have a noticeable impact on the SF for the simulated conditions.

4. Conclusions

2-D CFD simulations were performed of the VUCC of 8 mm diameter OFCu. A focused axisymmetric 2-D simulation was performed modelling the heat transported within the casting die for the inclusion of a 0.1 mm air gap, which typically formed between the solidified metal and the casting die. The results revealed a significant impact on the heat transported from the solidified OFCu into the super-cooler, with the overall effect being significantly greater heat remaining within the cast rod for longer as it was

VUCC, due to the presence of the air gap and a reduction in the heat transported as the rod is cast vertically.

Using data extracted from the heat transport simulation, another CFD simulation was performed of the crucible / die setup. Six different casting speeds were applied for VUCC and revealed that under equilibrium conditions, the heat extracted from the rod was greater for the slower speed resulting in lower temperatures within the rod. A region of continuous temperature was identified in the middle of the rod which was proportional to the casting speed. The temperature remained constant due to the latent heat of fusion solidification phenomena. Simulations of solidification showed that at slower speeds the lower temperatures produced a SF lower down within the rod, with complete solidification occurring lower in the die. The simulation model was validated from comparison with literature values of thermal measurements obtained from within the die.

A comparison between two casting conditions containing separately within their pulse cycle the motions pushback and dwell, highlighted that the copper microstructure altered in response to the applied motion and its impact on cast microstructure was predictable from the CFD simulations of the solidification front position. The developed model can be applied to provide insight into the casting behaviour for OFCu and with modification such as change in material parameters, can be applied to simulate alloys and used to predict cast outcomes and save on casting materials. The faster casting speeds produced high temperatures, higher up within the die which could act as an indicator for the occurrence of casting defects and will influence the final microstructure. The simulated conditions represent the latest state-of-the-art manufacturing conditions and due to the application of pushback, faster casting speeds can be achieved within manufacture.

The fluid flow magnitude and orientation were modelled in the simulation and showed that natural convection within the crucible was low relative to the motions within the casting die. As such, the fluid motions produced within the die were identified as contributing more to the solidification behaviour during VUCC than natural convection within the crucible.

Declaration of Competing Interest

The authors declare that they have no known competing financial interests or personal relationships that could have appeared to influence the work reported in this paper.

Acknowledgments

The authors thank Innovate UK for their financial support under grant project number 117521, as well as Rautomead Ltd for their advice and financial support.

Appendix A. Supplementary data

Supplementary data to this article can be found online at https://doi.org/10.1016/j.jestch.2020.12.009.

References

[1] Z. Sun, M. Guo, Y. Guo, Research of technological factors on producing oxygen-free copper strip in horizontal continuous casting, Adv. Mater. Res. 538–541 (2012) 1097–1100. doi:10.4028/www.scientific.net/AMR.538-541.1097.

[2] T. Knych, B. Smyrak, M. Walkowicz, Selected aspects of evolution properties of oxygen free copper for high-advanced electrotechnical application, Prz. Elektrotechniczny 87 (2011) 285–290. https://www2.scopus.com/inward/record.uri?eid=2-s2.0-81155137947&partnerID=40&md5=5d8d2c7111d5a1315050198 54f9f6113.

[3] H. Soda, G. Motoyasu, A. McLean, S.D. Bagheri, D.D. Perovic, Continuous casting of unidirectionally solidified copper rod, Int. J. Cast Met. Res. 9 (1) (1996) 37–44, https://doi.org/10.1080/13640461.1996.11819642.

[4] K. Härkki, J. Miettinen, Mathematical modeling of copper and brass upcasting, Metall. Mater. Trans. B 30 (1) (1999) 75–98, https://doi.org/10.1007/s11663-999-0009-6.

[5] E.-R. Bagherian, Y. Fan, M. Cooper, B. Frame, A. Abdolvand, Effect of water flow rate, casting speed, alloying elements and pull distance on tensile strength, elongation percentage and microstructure of continuous cast copper alloys, Metall. Res. Technol. 113 (3) (2016) 308, https://doi.org/10.1051/metal/2016006.

[6] E.-R. Bagherian, Y. Fan, M. Cooper, B. Frame, A. Abdolvand, Effect of melt temperature, cleanout cycle, continuous casting direction (horizontal / vertical) and super-cooler size on tensile strength, elongation percentage and microstructure of continuous cast copper alloys, Metall. Res. Technol. 113 (2016) 502, https://doi.org/10.1051/metal/2016030.

[7] N. Muramatsu, M. Akaiwa, Characteristics of hypoeutectic Cu–Zr alloy rods manufactured by vertically upwards continuous casting, Mater. Trans. 57 (10) (2016) 1794–1800, https://doi.org/10.2320/matertrans.M2016181.

[8] E.-R. Bagherian, Y. Fan, M. Cooper, B. Frame, A. Abdolvand, Investigation of the distribution of lead in three different combinations of brass feedstock, Int. Metalcast. 10 (3) (2016) 322–328, https://doi.org/10.1007/s40962-016-0055-1.

[9] E.R. Bagherian, C. Bell, M. Cooper, Y.C. Fan, B. Frame, M. Rose, Analysis and quantification of grain size of various DHP copper tubes manufacturing processes, Adv. Mater. Res. 856 (2014) 241–245. doi:10.4028/www.scientific.net/AMR.856.241.

[10] D. Mackie, J.D. Robson, P.J. Withers, M. Turski, Characterisation and modelling of defect formation in direct-chill cast AZ80 alloy, Mater. Charact. 104 (2015) 116–123, https://doi.org/10.1016/j.matchar.2015.03.033.

[11] T. Nozaki, S. Itoyama, Horizontal continuous casting processes. The state of the art and future trends., ISIJ Int. 27 (5) (1987) 321–331, https://doi.org/10.2355/isijinternational1966.27.321.

[12] K. Nakai, Y. Umeda, Y. Sugitani, M. Miura, Effects of factors on the stability of casting in horizontal continuous casting., ISIJ Int. 24 (11) (1984) 983–991, https://doi.org/10.2355/isijinternational1966.24.983.

[13] T.D.A. Jones, A. Bernassau, D. Flynn, D. Price, M. Beadel, M.P.Y. Desmulliez, Copper electroplating of PCB interconnects using megasonic acoustic streaming, Ultrason. Sonochem. 42 (2018) 434–444, https://doi.org/10.1016/j.ultsonch.2017.12.004.

[14] T.D.A. Jones, A. Bernassau, D. Flynn, D. Price, M. Beadel, M.P.Y. Desmulliez, Analysis of throwing power for megasonic assisted electrodeposition of copper inside THVs, Ultrasonics 104 (2020) 106111, https://doi.org/10.1016/j.ultras.2020.106111.

[15] B.G. Thomas, L. Zhang, Mathematical modeling of fluid flow in continuous casting, ISIJ Int. 41 (2001) 1181–1193, https://doi.org/10.2355/isijinternational.41.1181.

[16] T. Jones, J. Vorstius, D. Mackie, R. Strachan, M. Cooper, B. Frame, Optimising computational fluid dynamic conditions for simulating copper vertical casting, BT-Mater. Sci. For. 1106 (2020) 642–647. https://www.scientific.net/MSF.

[17] Z.Y. Ahmad, T.A.L. Harris, The effect of solidification on the casting window after bubble entrainment, J. Coat. Technol. Res. 11 (1) (2014) 89–93, https://doi.org/10.1007/s11998-013-9502-6.

[18] M. Thompson, J. Thompson, Considerations for predicting thermal contact resistance in ANSYS, Ansys (2007).

[19] J.R. Davis, A.S.M.I.H. Committee, Copper and Copper Alloys, ASM International, 2001. https://books.google.co.uk/books?id=sxkPJzmkhnUC.

[20] B.J. Florio, M. Vynnycky, S.L. Mitchell, S.B.G. O'Brien, Mould-taper asymptotics and air gap formation in continuous casting, Appl. Math. Comput. 268 (2015) 1122–1139, https://doi.org/10.1016/j.amc.2015.07.011.

[21] M. Sheikholeslami, M. Jafaryar, Ahmad Shafee, Houman Babazadeh, Acceleration of discharge process of clean energy storage unit with insertion of porous foam considering nanoparticle enhanced paraffin, J. Cleaner Prod. 261 (2020) 121206, https://doi.org/10.1016/j.jclepro.2020.121206.

[22] M. Sheikholeslami, A. Nematpour Keshteli, Houman Babazadeh, Nanoparticles favorable effects on performance of thermal storage units, J. Mol. Liq. 300 (2020) 112329, https://doi.org/10.1016/j.molliq.2019.112329.

[23] V.E. Bazhenov, A.V. Koltygin, Yu.V. Tselovalnik, A.V. Sannikov, Determination of interface heat transfer coefficient between aluminum casting and graphite mold, Russ. J. Non-ferrous Metals 58 (2) (2017) 114–123, https://doi.org/10.3103/S1067821217020031.

[24] ASTM International, ASTM E112-13, Standard Test Methods for Determining Average Grain Size, 2013. www.astm.org/cgi-bin/resolver.cgi?E112.

[25] F. Menter, Zonal two equation k-w turbulence models for aerodynamic flows, in: 23rd Fluid Dyn. Plasmadynamics, Lasers Conf., American Institute of Aeronautics and Astronautics, 1993. doi:doi:10.2514/6.1993-2906.

[26] Peri Subrahmanya Srinivas, Deepak Kumar Mishra, Akshay Bandopant Kulkarni, Raghvendra Gupta, Jose Martin Korath, Amiya Kr Jana, Investigation of vortex flow patterns at the meniscus in a water caster mould, Can. Metall. Q. 59 (2) (2020) 211–232, https://doi.org/10.1080/00084433.2020.1727128.

[27] Zhi Tao, Zeyuan Cheng, Jianqin Zhu, Haiwang Li, Effect of turbulence models on predicting convective heat transfer to hydrocarbon fuel at supercritical pressure, Chin. J. Aeronaut. 29 (5) (2016) 1247–1261, https://doi.org/10.1016/j.cja.2016.08.007.

[28] L. Nastac, K. Pericleous, A.S. Sabau, L. Zhang, B.G. Thomas, CFD Modeling and Simulation in Materials Processing 2018, Springer International Publishing (2018), https://doi.org/10.1007/978-3-319-72059-3.

[29] C. Prakash, M. Samonds, A.K. Singhal, A fixed grid numerical methodology for phase change problems involving a moving heat source, Int. J. Heat Mass

Transf. 30 (12) (1987) 2690–2694, https://doi.org/10.1016/0017-9310(87)90152-9.
[30] A. Neale, D. Derome, B. Blocken, J. Carmeliet, Determination of surface convective heat transfer coefficients by CFD, NBEC (2007).
[31] L.C. Thomas, Heat Transfer, Prentice Hall, 1992. https://books.google.co.uk/books?id=Hq2mQgAACAAJ.
[32] J.A. Cahill, A.D. Kirshenbaum, The density of liquid copper from its melting point (1356°K.) to 2500°K and an estimate of its critical constants1,2, J. Phys. Chem. 66 (1962) 1080–1082. doi:10.1021/j100812a027.
[33] M. Uoti, M. Immonen, K. Härkki, Theoretical and experimental study of vertical continuous casting of copper, Contin. Cast. (2000) 143–148, https://doi.org/10.1002/3527607331.ch21.
[34] Z.Z. Cai, M.Y. Zhu, Simulation of air gap formation in slab continuous casting mould, Ironmaking Steelmaking 41 (6) (2014) 435–446, https://doi.org/10.1179/1743281213Y.0000000139.
[35] M. Bamberger, B. Prinz, Determination of heat transfer coefficients during water cooling of metals, Mater. Sci. Technol. 2 (4) (1986) 410–415, https://doi.org/10.1179/mst.1986.2.4.410.
[36] J. Campbell, Complete Casting Handbook: Metal Casting Processes, Techniques and Design, Elsevier Science, 2011. https://books.google.co.uk/books?id=PJduV5ShuSIC.
[37] P.H. Zhang, R.Z. Chang, Z. Wei, H. Cao, X.N. Zhou, The melting point, latent heat of solidification, and enthalpy for both solid and liquid α-Al2O3 in the range 550–2400 K, Int. J. Thermophys. 7 (1986) 811–819, https://doi.org/10.1007/BF00503838.
[38] V.Ya. Chekhovskoi, V.D. Tarasov, Yu.V. Gusev, Calorific properties of liquid copper, High Temp. 38 (3) (2000) 394–399, https://doi.org/10.1007/BF02755998.
[39] S.I. Ao, H.K. Kim, M.A. Amouzegar, Transactions on Engineering Technologies: World Congress on Engineering and Computer Science 2015, in, Springer Singapore, 2017.
[40] K. Liu, C. Wang, G. Liu, D. Ning, S. Qi-song, Zhi-hongTian., Research on soft reduction amount distribution to eliminate typical inter-dendritic crack in continuous casting slab of X70 pipeline steel by numerical model, High Temp. Mater. Process. 36 (2017) 359–372. doi:doi:10.1515/htmp-2016-0160.
[41] Suyitno, V.I. Savran, L. Katgerman, D.G. Eskin, Effects of alloy composition and casting speed on structure formation and hot tearing during direct-chill casting of Al-Cu alloys, Metall. Mat. Trans. A 35 (11) (2004) 3551–3561, https://doi.org/10.1007/s11661-004-0192-7.
[42] A. Sergejevs, A. Kromanis, J. Ozolins, E. Gerins, Influence of casting velocity on mechanical properties and macro-structure of tin bronzes, Key Eng. Mater. 674 (2016) 81–87. doi:10.4028/www.scientific.net/KEM.674.81.
[43] R.V. Gavrilova, V.B. Hadzhiyski, M.K. Mihovsky, Structure and mechanical properties of vertical upwards continuously casted aluminium wires, Struct. Integr. Life. 10 (2010) 219–223. http://divk.inovacionicentar.rs/ivk/ivk10/ivk1003-9.html.
[44] D.A. Porter, K.E. Easterling, Phase Transformations in Metals and Alloys, Third Edition (Revised Reprint), Taylor & Francis, 1992. https://books.google.co.uk/books?id=eYR5Re5tZisC.
[45] M. Wu, M. Ahmadein, A. Ludwig, Premature melt solidification during mold filling and its influence on the as-cast structure, Front. Mech. Eng. 13 (1) (2018) 53–65, https://doi.org/10.1007/s11465-017-0437-y.
[46] Nilanjan Chakraborty, The effects of turbulence on molten pool transport during melting and solidification processes in continuous conduction mode laser welding of copper–nickel dissimilar couple, Appl. Therm. Eng. 29 (17-18) (2009) 3618–3631, https://doi.org/10.1016/j.applthermaleng.2009.06.018.